Authors:
Enrico Canuto, Wilber Acuña-Bravo, Carlo Perez Montenegro

Affiliation:
Politecnico di Torino, Dipartimento di Automatica e Informatica
Corso Duca degli Abruzzi 24, 10129 Torino, Italy

enrico.canuto@polito.it
wilber.acaunabravo@polito.it
carlos.perez@polito.it

Biographical statements

Enrico Canuto
Enrico Canuto was born in Varallo (Piemonte), Italy. He received a degree in Electrical Engineering from Politecnico di Torino, Turin, Italy, where he joined the staff as Associate Professor of Automatic Control in 1983. From 1982 to 1997 he contributed to data reduction of the European astrometric mission Hipparcos. Technological studies in view of scientific and drag-free space missions, like Gaia and GOCE provided the opportunity of applying Embedded Model Control to drag-free satellites and to electro-optics. He contributed to the conception, design and implementation of the Nanobalance interferometric thrust-stand, capable of sub-micronewton accuracy. Presently he is involved in the design of the orbit, formation and attitude control of the Next Generation Gravity Missions of the European Space Agency. His research interests cover all the entire field of control problems that are challenging because of complexity, uncertainty and precision.

Wilber Acuña-Bravo
Wilber Acuña-Bravo was born in Mérida, Venezuela, in 1980. He received a degree in Electrical Engineering from Universidad del Quindío, Armenia, Colombia, and a M.S. degree in Control Engineering from Universidad de Los Andes, Mérida, Venezuela. In 2011 he received the Ph.D. degree in Information and System Engineering from Politecnico di Torino, Turin, Italy, where he is currently research assistant. His research interests include electro-hydraulic control systems and control applications.

Carlo Perez Montenegro
Carlos Perez Montenegro was born in Santa Fé de Bogotá, Colombia, in 1983. In 2007 he received a degree in Electrical Engineering from Pontificia Universidad Javeriana, Bogotá, Colombia. Currently he is a Ph. D. student in Information and System Engineering at Politecnico di Torino, Turin, Italy. His main research interests include space control applications and quadricopter design and control

Published by Int. J. Mechatronics and Automation, Vol. 3, No. 2, 2013, pp.94-109

Robust control stability using the error loop

Abstract - The paper formulates the error loop as a tool for designing robust stability control systems in the presence of structured and unstructured uncertainties. The error loop indicates that uncertainties can be accommodated through the design of the noise estimator, which is the unique feedback channel from plant to control. The real-time model that is embedded in the control unit and the noise estimator constitutes a state predictor. The embedded model consists of a controllable dynamics plus a disturbance dynamics fed by the noise estimator. It is shown that causality constraint prevents perfect cancellation of causal uncertainties (unknown disturbance), but makes the control law which is fed by the state predictor to play a role, thus offering a further degree of freedom. Employing asymptotic expansions of the closed-loop transfer functions, simple, explicit design formulae derive from stability inequalities. They relate closed-loop eigenvalues to model parameters and requirements, and define an admissible frequency band for the state predictor bandwidth. The paper restricts formulation to the univariate case. A simple example is provided with simulated and experimental data.

Key words - Robust control, closed-loop, stability, error loop, embedded model control.

1. Introduction

1.1. Uncertainty and the error loop

Closed-loop performance is affected by uncertain discrepancies between model and reality. Three kinds of discrepancies may be distinguished (Maciejowski, 1989, and Doyle, Francis and Tannenbaum, 1992) as in Figure 1.

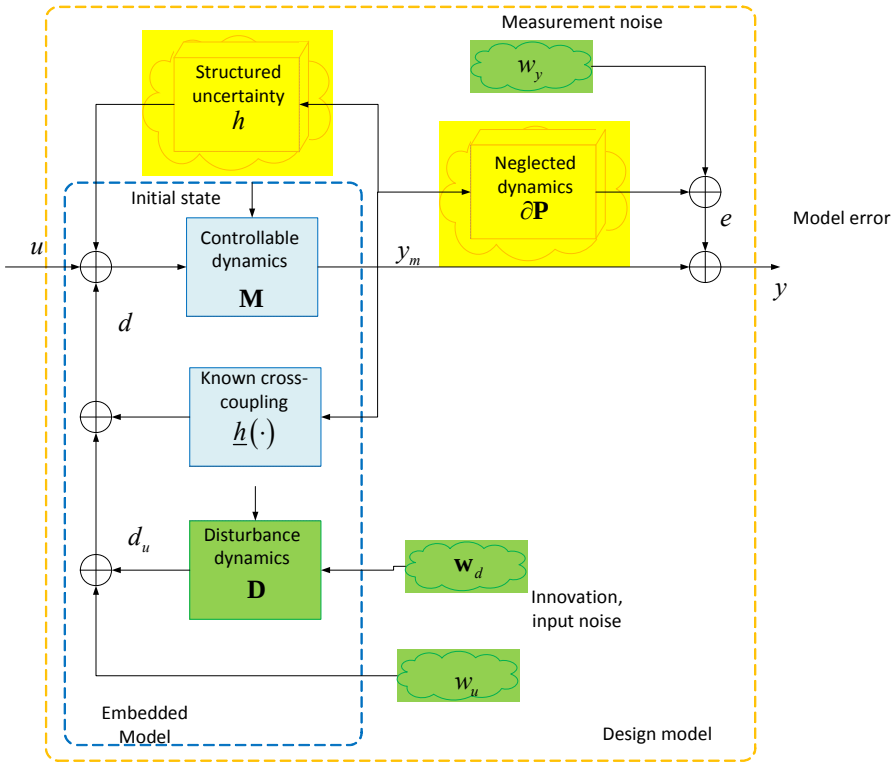

Figure 1 Block-diagram of embedded model and uncertainties.

Causal uncertainty, denoted by clouds, regards unpredictable actions, referred to as innovation, and formulated either as a white-noise or a bounded and arbitrary-signal class corresponding to $\mathbf{w}_d$ and w_u in Figure 1. They are independent of the model state and command and only affect performance. The mechanism through which they affect a plant is not merely unpredictable, as they accumulate prior to be released. Causes of this kind are referred to as 'unknown' disturbance and their model, the disturbance dynamics $\mathbf{D}$ in Figure 1, generates the signal class $d_u \in \mathcal{D}_u$. The control goal is to cancel their effect less the innovation, as the latter occurs while the command is acting on the plant. Innovations $\mathbf{w}_d$ and w_u are necessary and sufficient for updating the state of $\mathbf{D}$. They must be real-time estimated by correlating them to the model error $e = y - y_m$ through a noise estimator as in Canuto, Molano and Massotti (2010). This is the basic mechanism of the 'disturbance observers' pioneered by Johnson (1971) and Hostetter and Meditch (1973), and further studied and applied by Mita, Hirata, Murata and Zhang (1998), Bickel and Tomizula (1999), Schrijver and van Dijk (2002), Choi, Yang, Chung, Kim and Suh (2003), Katsura, Matsumoto and Ohnishi (2007). The Embedded Model Control of Canuto (2007) inspired by Donati and Vallauri (1984) develops around the concept that noise is the necessary and sufficient feedback from plant to control. The ensemble of noise estimator and design model, to be embedded as a real-time model in the control unit - hence the name embedded model - implements a one-step state predictor.

The structured (or parametric) uncertainty $h(\cdot)$, denoted by a cloudy 3D box, either refers to discrepancies from the model class in the form of parameter uncertainty or to neglected relations between model variables (cross couplings). They must be distinguished from the known interconnections, that are denoted with $\underline{h}(\cdot)$ and must be treated as known disturbances. They have been extensively studied in the literature, as for instance by Chapellat, Dahleh and Bhattacharyya (1990), Foo and Soh (1993), Ross Barmish (1994), Calafiore and Dabbene (2002), Chen, Chou and Zheng (2005), Patre, MacKunis, Makkar and Dixon (2008). They may take several forms, from command-to-state to output-to state relations: only state-to-command relations are treated here since they affect the model eigenvalues. They are included in the so-called design model and implemented as a numerical simulator, but they are forcedly neglected in the embedded model, except for the known part $\underline{h}$, and are surrogated by the unknown disturbance class $\mathcal{D}_u$. The advantage is that h can be made implicitly known by d_u and therefore cancelled by u, thus favouring robustness of the model-based design since model-plant discrepancies encoded in e are attenuated. The difficulty is that h, being output and command dependent cannot belong to $\mathcal{D}_u$, as the latter is defined as a class of command independent signals. This is one of the chief instability sources of any feedback control design, since feedback signals – in this case the estimated innovations $\mathbf{w}_d$ and w_u - spill components incoherent with the design model. Appropriate stability conditions need to be formulated and proved, which are shown to be mainly related to the noise estimator (and therefore to the state predictor) design. Specifically, frequency-domain design suggests to enlarge the state predictor bandwidth (BW) to allow estimation and cancellation of the dominant low frequency components.

Unstructured uncertainty, denoted by a cloudy 3D box, refers to model-class discrepancies and uncertainties, which are unavoidable due to the embedded model finite order. They may take several forms as in Maciejowski (1989), Doyle, Francis and Tannenbaum (1992) and Ross Barmish (1994). The output fractional form (multiplicative form in Doyle, Francis and Tannenbaum, 1992) is adopted here as

in Canuto (2007) and in Canuto, Acuna-Bravo, Molano and Perez (2012). They are driven by the model output y_m and yield the model error e (plant minus model) as output, as follows

$$e = y - y_m = \partial\mathbf{P}(y_m) + w_y, \tag{0}$$

where y is the measured plant output. The dynamic operator $\partial\mathbf{P}$ is the (uncertain) 'neglected dynamics', a term preferable to unstructured uncertainty, and w_y is the measurement error, which has been assumed adding to $\partial\mathbf{P}$. Components of (1) are completely neglected in the embedded model. Spilling e to the command through feedback must be restricted, since, for what concerns $\partial\mathbf{P}$, it can be assimilated to a command-dependent output error. In addition w_y prevents accurate estimation of the innovations $\mathbf{w}_d$ and w_u, which difficulty leads to Kalman filter optimization (see Kwakernaak and Sivan, 1972). The uncertainty based design imposes to avoid noise estimation in the frequency band (usually at higher frequencies below Nyquist frequency) where $\partial\mathbf{P}$ dominates.

As a result in robust design, structured and unstructured uncertainties must be accommodated by a trade-off in the design of the state predictor bandwidth: a wider band is required to cancel structured discrepancies, a narrower band to prevent spilling of neglected dynamics. The design defines a stability interval where to place noise-estimator gains or, equivalently, the state-predictor eigenvalues. Converting eigenvalues into frequency domain, lower and upper bounds of the state-predictor bandwidth are obtained. The interval width depends on the ratio of the predictor and control-law eigenvalues, and on a stability margin. When the interval is void, robust design becomes unfeasible, which may be due to excessive stability margin (conservative design) or large uncertainty (poor modelling).

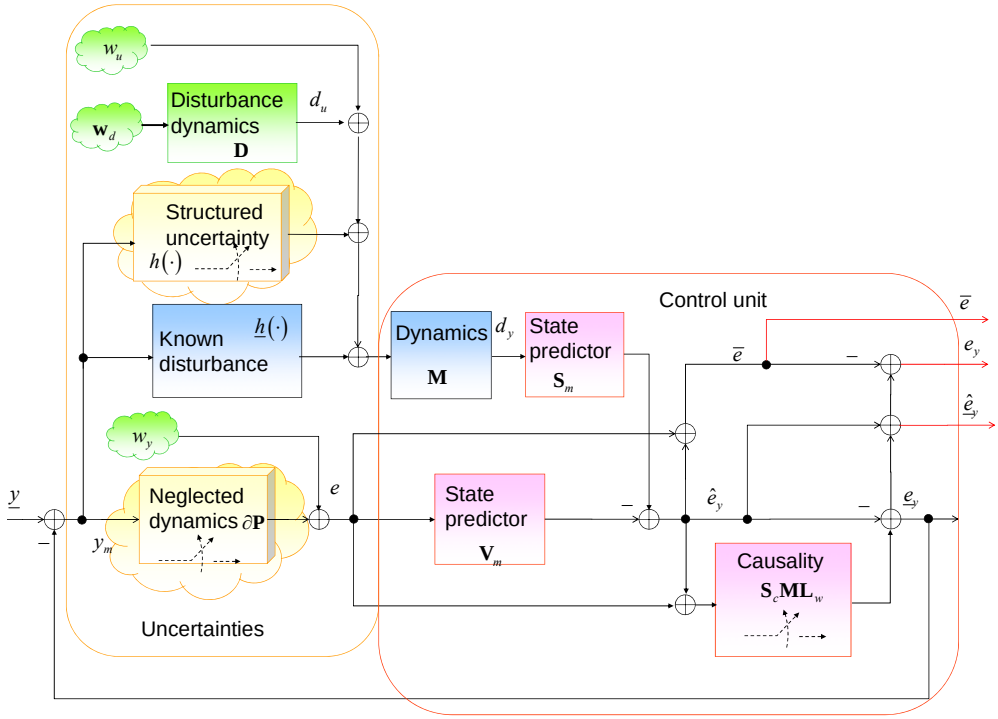

Figure 2 Block-diagram of the error loop.

Stability inequalities are obtained in Section 3 from error equations driven by model uncertainties in Figure 1. They generate a loop passing through different errors, and therefore designated as the 'error

loop' in Canuto (2007). Three main errors enter the loop in Figure 2: the model error e defined in (1), the tracking error $\underline{e}_y$ and the prediction error $\hat{e}_y$ defined by

$$\begin{aligned} \underline{e}_y &= \underline{y} - y_m \\ \hat{e}_y &= y_m - \hat{y}_m \end{aligned}, \tag{0}$$

where $\underline{y}$ is the reference signal driving the loop and $\hat{y}_m$ is the one-step prediction of the model output y_m. None of the above errors is measurable as they include the model output y_m, which is only available either as a signal class or from simulated runs. The corresponding measurable errors that are indicated as the output of the control unit in Figure 2, are made available by replacing y_m either with $\hat{y}_m$ or $\underline{y}$ in (2). They correspond to the measured model error $\overline{e}$, to the measured tracking error $\underline{\hat{e}}_y$ and to the control error e_y. They are defined as follows

$$\begin{aligned} \overline{e} &= y - \hat{y}_m = e + \hat{e}_y \\ \underline{\hat{e}}_y &= \underline{y} - \hat{y}_m = \underline{e}_y + \hat{e}_y \\ e_y &= \underline{y} - y = \underline{\hat{e}}_y - \overline{e} = \underline{e}_y - e \end{aligned} \quad . \tag{1}$$

1.2. Content of the paper

In Section 3 the paper concentrates on the derivation and properties of the error loop. The main result is the following: structured and unstructured uncertainties may be accommodated by the state predictor sensitivity $\mathbf{S}_m$ and its complement $\mathbf{V}_m$ as shown in Figure 2. The result seems partly departing from most of the literature, where either the control law is dedicated to the purpose as in Solihin, Akmeliawati and Legowo (2011) or no distinction between control and state predictor is made. On the contrary, structured uncertainties must be real-time estimated so as to update the embedded model. This is obtained by shaping the lower-frequency part of the sensitivity $\mathbf{S}_m$. Unstructured uncertainties must be blocked from spilling into the embedded model in order to prevent instability. This is achieved by shaping the higher-frequency part of $\mathbf{V}_m$. Actually, as shown in Section 3, because of causality, which prevents cancelling innovation w_u in Figure 1, – w_u and $\mathbf{w}_d$ can only be causally estimated –, the state predictor is affected by the correction $\mathbf{S}_w = \mathbf{S}_c\mathbf{M}\mathbf{L}_w\mathbf{S}_m$ in Figure 2, right bottom, which depends on the control-law sensitivity $\mathbf{S}_c$, the controllable dynamics $\mathbf{M}$ and the noise estimator $\mathbf{L}_w$. Causality adds a degree of freedom and shows how state predictor and control law intertwine in the overall control sensitivity $\mathbf{S}$ and its complement $\mathbf{V}$.

Shaping $\mathbf{S}_m$ and $\mathbf{S}$ is done by approximating them and their complements $\mathbf{V}_m$ and $\mathbf{V}$ with low- and high-frequency asymptotes, respectively, within the Nyquist frequency band. Asymptotes can be related to noise estimator and control gains and to state predictor and state feedback eigenvalues. The intercept of the asymptotes with the zero dB line is interpreted as the (asymptotic) sensitivity and complement bandwidths. The main results is that a robust design accommodating structured and unstructured uncertainty defines an admissible region Δf_m of the bandwidth f_m of the state predictor sensitivity $\mathbf{S}_m$. The admissible region in turn depends on the control ratio $\gamma = f_m / f_c$, f_c being the bandwidth of $\mathbf{S}_c$, and on the stability margin $\eta^{-1} > 1$. Machinery and proof of the asymptotes are carried out step by step throughout the paper.

Main contributions are credited to be (i) the modelling procedure pivoting on the disturbance dynamics $\mathbf{D}$ and on the driving noise as the sole plant-to-model feedback, (ii) the performance equation (63) including all the uncertainty contributions and their closed-loop accommodating filters, (iii) the derivation of (63) in Section 3, (iv) the asymptotic inequalities in Section 3 and their derivation throughout the paper. More sophisticated algorithms, simulation and in-field tuning may refine the resulting robust design.

Formulation employs discrete-time transfer functions denoted as $y(z)=\mathbf{M}(z)u(z)$. Sometimes z is dropped. Since the paper aims to be introductory, the univariate case is treated.

2. The embedded model and the uncertainty

2.1. The embedded model and its realization

2.1.1. Generalities

A discrete-time dynamics is considered, which is associated to the time unit T, to the Nyquist frequency $f_{\max}=0.5/T$ and to discrete times iT. The model output y_m is the response to the command u and to the disturbance d as follows (see Figure 1)

$$\begin{aligned} y_m(z) &= \mathbf{M}(z)\big(u(z)+d(z)\big)=\mathbf{M}(z)u(z)+d_y(z) \\ d(z) &= d_u(z)+w_u(z)+h(\mathbf{x}_c)+\underline{h}(\mathbf{x}_c) \end{aligned}, \tag{1}$$

where

$$\mathbf{M}=C_c(zI-A_c)^{-1}B_c=C_cN(z)/\phi(z) \tag{1}$$

is irreducible and of order n_c. To be simple, $C_cN(z)$ is assumed to be Hurwitz. The input signals u and d are scaled to the output units; d_y is the output disturbance to be used in Section 3. The disturbance d is decomposed into the following components:

1) The unknown disturbance $d_u(z)=\mathbf{D}(z)\mathbf{w}_d(z)$ is driven by a noise vector $\mathbf{w}_d$ of size n_w through the irreducible dynamics $\mathbf{D}=M_c(zI-A_d)^{-1}G_d$ of order n_d, with state vector $\mathbf{x}_d$. The disturbance must be rejected by the control action.
2) The unpredictable noise $w_u(z)$ cannot be cancelled due to causality, since any sample $w_u(i)$ occurs while the command sample $u(i)$ actuates plant and model.
3) The nonlinear feedback $h(\mathbf{x}_c)+\underline{h}(\mathbf{x}_c)$ depends on the state $\mathbf{x}_c$ of $\mathbf{M}$; the unknown part $h(\mathbf{x}_c)$ is treated as a structured uncertainty to be estimated and rejected by the control action.

The disturbance dynamics $\mathbf{D}$ plays the role of the weighting functions in Maciejowski (1989) and Doyle, Francis and Tannenbaum, (1992), but is designed to be parameter-free and explicitly coded in the control unit. A disturbance adding to the command is the simplest case, which is referred to as the collocated case. The not collocated case is treated in Canuto (2007). Signals $\mathbf{w}_d$ and w_u may be treated as white noise, but when statistics is unknown they may be also interpreted as bounded, arbitrary signals, whose average converges to a null value. Null value is therefore their best prediction.

All the state variables of $\mathbf{M}$ and $\mathbf{D}$ are observable by the model output y_m. Low- and high-frequency asymptotes of $\mathbf{M}$ for $f<f_{\max}$ are as follows

$$\begin{aligned} &\lim_{f\to 0}\left|\mathbf{M}\left(jf\right)\right| = \left(f_0 / f\right)^{m_0} \\ &\lim_{|f|\to\infty<f_{\max}}\left|\mathbf{M}\left(jf\right)\right| = \left(f_\infty / f\right)^{m_\infty} \end{aligned}, \tag{1}$$

where $m_0 > 0$ and $m_\infty > 0$ imply a pole-zero excess of at least one. Since $\mathbf{D}$ is sized $1\times n_w$, it is post-multiplied times the arbitrary transfer vector $\mathbf{L}_d\left(z\right)$, $n_w \times 1$, in a way that no zero-pole cancellation occurs, and

$$\begin{aligned} &\lim_{z\to 1}\mathbf{L}_d\left(z\right) = L_{d0} < \infty \\ &\lim_{z\to\infty}\mathbf{L}_d\left(z\right) = L_{d\infty} < \infty \end{aligned}. \tag{2}$$

Then, given $\mathbf{L}_d\left(z\right)$ satisfying (7), we assume

$$\begin{aligned} &\lim_{f\to 0}\left|\mathbf{M}\left(jf\right)\mathbf{D}\left(jf\right)\mathbf{L}_d\left(jf\right)\right| = \left(f_{d0} / f\right)^{d_0} \\ &\lim_{|f|\to\infty<f_{\max}}\left|\mathbf{M}\left(jf\right)\mathbf{D}\left(jf\right)\mathbf{L}_d\left(jf\right)\right| = \left(f_{d\infty} / f\right)^{d_\infty} \end{aligned}, \tag{3}$$

where $d_0 - m_0 > 0$ and $d_\infty - m_\infty > 0$ imply that $\mathbf{DL}_d$ possesses at least a unitary pole. The $\lim_{|f|\to\infty<f_{\max}}$ accounts for asymptotes in the region $f < f_{\max}$: they are due to poles in excess of the type $\left(z-1+\beta\right)^{-1}$ with $0 \le \beta < 1$, and thus exclude pure delays.

The noise $\mathbf{w}_d$ is multivariate, since $\mathbf{D}$ is the composition of different stochastic signals, and each component is driven by different noise components. Moreover $\mathbf{M}$ and $\mathbf{D}$ are assumed to be strictly causal, which implies that the relevant output y_m and d_u are a linear combination of state vectors only. $\mathbf{D}$ is usually stylized from experimental spectral densities by whitening their perturbing sources as in Canuto and Rolino (2004) and Canuto (2008). The Embedded Model Control implements the control unit around equation (4) written in the form of a state equation. This entails the need of estimating the noise vectors $\mathbf{w}_d\left(i\right)$ and $w_u\left(i\right)$ for updating controllable and disturbance states. As in Kalman filtering (see Kwakernaak and Sivan, 1972) the only way to the purpose is to extract the causal estimates $\overline{\mathbf{w}}$ and $\overline{w}_u$ from the model error e defined in (1).

2.1.2. Example

Consider a balanced robot arm moving, in a vertical plane, a mass m that is distant l from the rotation centre. The counter-clockwise rotation θ with respect to the horizontal plane is denoted with y_m. The angular rotation $\omega = \dot{y}_m$ is replaced by the angular increment $\Delta\theta = \omega T$. The arm is driven by a DC motor and is subject to gravity torque and friction. The total inertia on the gear output shaft is J. Gear backlash and torsional deformation are confined into neglected dynamics, as well as amplifier dynamics and LuGre friction dynamics (Canudas de Wit, Olsson, Åström and Lischinsky, 1995). Transfer functions and $h\left(\cdot\right)$ in (4) hold

$$\mathbf{M}(z)=(z-1)^{-2},\ \mathbf{x}_c=\begin{bmatrix} y_m=\theta \\ \Delta\theta \end{bmatrix}$$
$$\mathbf{D}(z)\mathbf{w}_d(z)=(z-1)^{-1}\begin{bmatrix}1 & (z-1)^{-1}\end{bmatrix}\begin{bmatrix} w_a \\ w_s \end{bmatrix}(z),\ \mathbf{x}_c=\begin{bmatrix} a \\ s \end{bmatrix}. \tag{3}$$
$$h(\mathbf{x}_c)=-\left(\operatorname{sgn}(\Delta\theta)A(|\Delta\theta|)-mgl\cos(y_m)\right)T^2/J$$
$$\underline{h}(\mathbf{x}_c)=0$$

Parameters in (6) can be proved to hold

$$m_0=m_\infty=2,\ d_0=d_\infty=4$$
$$f_0=f_\infty=f_{d0}=f_{d\infty}=(2\pi T)^{-1}. \tag{3}$$

The block diagram with input, state and output variables is in Figure 3. The noise size is $n_w=3$ and the embedded model size parameters are $n=d_0=d_\infty=4$. The block-diagram includes the reference dynamics to be explained in Section 2.3. Boxes marked with Σ represent discrete-time integrators having the generic state equation

$$x(i+1)=x(i)+u(i),\ x(0)=x_0. \tag{4}$$

Initial states are marked by a superimposed arrow.

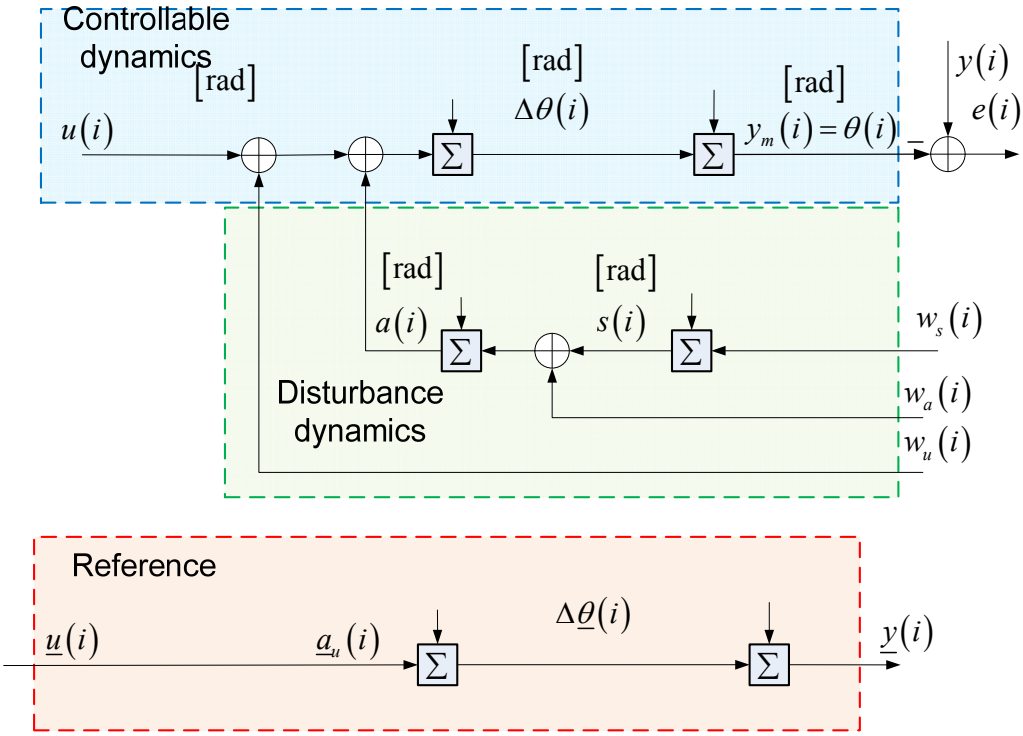

Figure 3 Block dagram of the Embedded Model of the example.

Similar design model and considerations apply to a ball and beam device (Keshmiri, Jahromi, Mohebbi, Amoozgar and Xie, 2012), when ball position is uncontrolled. The ball control would require a more complex dynamics than (9).

2.2. Noise estimation and output prediction

2.2.1. Generalities

Noise estimation forces the embedded model to update and instantiate the signals $y_m(i)$ and $d_u(i)$ into the realizations $\hat{y}_m(i)$ and $\hat{d}_u(i)$. The mark ^ denotes one-step prediction as the relevant signals only depend on the past measures $y(i-k),\ k>0$. On the contrary, the noise estimates $\overline{\mathbf{w}}_d(i)$ and $\overline{w}_u$, and the actual (or measured) model error $\overline{e}(i)=y(i)-\hat{y}_m(i)$ are barred, meaning they depend on the present measure $y(i)$. Thus one must distinguish between the a priori embedded model (4) and the a posteriori model which is implemented in the control unit and is forced by a realization $\overline{e}$ of e. Consequently, unknown prediction errors establish between model signals and their prediction as follows

$$\begin{aligned}\hat{e}_y &= y_m-\hat{y}_m\\ \hat{e}_d &= d_u+h(\mathbf{x}_c)-\hat{d}_u\end{aligned}. \tag{4}$$

Defining the noise error as $\overline{e}_w=w_u-\overline{w}_u$, a first expression relating $\hat{e}$ to the errors in (12) is

$$\hat{e}_y(z)=\mathbf{M}(z)\left(\hat{e}_d+\overline{e}_w\right)(z). \tag{4}$$

To prove it, with the help of (4), rewrite the former equation in (12) as follows

$$y_m-\hat{y}_m=\mathbf{M}\left(u+d_u+w_u+h(\mathbf{x}_c)+\underline{h}(\mathbf{x}_c)\right)-\mathbf{M}\left(u+\hat{d}_u+\overline{w}_u+\underline{h}(\mathbf{x}_c)\right). \tag{5}$$

Equation (14) yields (13) with the help of the second equation in (12).

A further expression derives from the linear and time-invariant noise-estimator, which is driven by the measured model error $\overline{e}$ and is partitioned as follows

$$\begin{aligned}\overline{\mathbf{w}}_d(z)&=\mathbf{L}_d(z)\overline{e}(z)\\ \overline{w}_u(z)&=\mathbf{L}_w(z)\overline{e}(z)\end{aligned}, \tag{5}$$

where $\mathbf{L}_d$ and $\mathbf{L}_w$ are suitable transfer functions having finite gains for $z\to 1$ and $z\to\infty$, i.e.

$$\begin{aligned}\lim_{z\to 1}\mathbf{L}_w(z)&=l_{w0}\\ \lim_{z\to\infty}\mathbf{L}_w(z)&=l_{w\infty}\end{aligned}. \tag{6}$$

Specifically $\mathbf{L}_w$ must be all-pass for estimating the white noise w_u, whereas $\mathbf{L}_d$ may be low-pass. Replacing (15) in (13) and dropping z yields

$$\begin{aligned}\hat{e}&=\mathbf{M}\left(h(\mathbf{x}_c)+d_u+w_u+\underline{h}(\mathbf{x}_c)\right)-\mathbf{M}\left(\mathbf{D}\mathbf{L}_d+\mathbf{L}_w\right)\overline{e}=\\ &=d_y-\mathbf{M}\mathbf{H}\hat{e}-\mathbf{M}\mathbf{H}e\end{aligned}, \tag{6}$$

where the output disturbance d_y in (4) has been used together with the overall feedback $\mathbf{H}=\mathbf{DL}_d+\mathbf{L}_w$ and the key error equality

$$\overline{e}=e+\hat{e}_y\,. \tag{7}$$

Assumptions on $\mathbf{L}_d$ and $\mathbf{L}_w$ imply $\mathbf{H}$ to be proper. Inserting the sensitivity $\mathbf{S}_m=(1+\mathbf{MH})^{-1}$ and the complement $\mathbf{V}_m=1-\mathbf{S}_m$ into (17), yields the second expression of $\hat{e}$, namely

$$\hat{e}_y(z)=-\mathbf{V}_m(z)e(z)+\mathbf{S}_m(z)d_y(z), \tag{7}$$

which is illustrated in Figure 2.

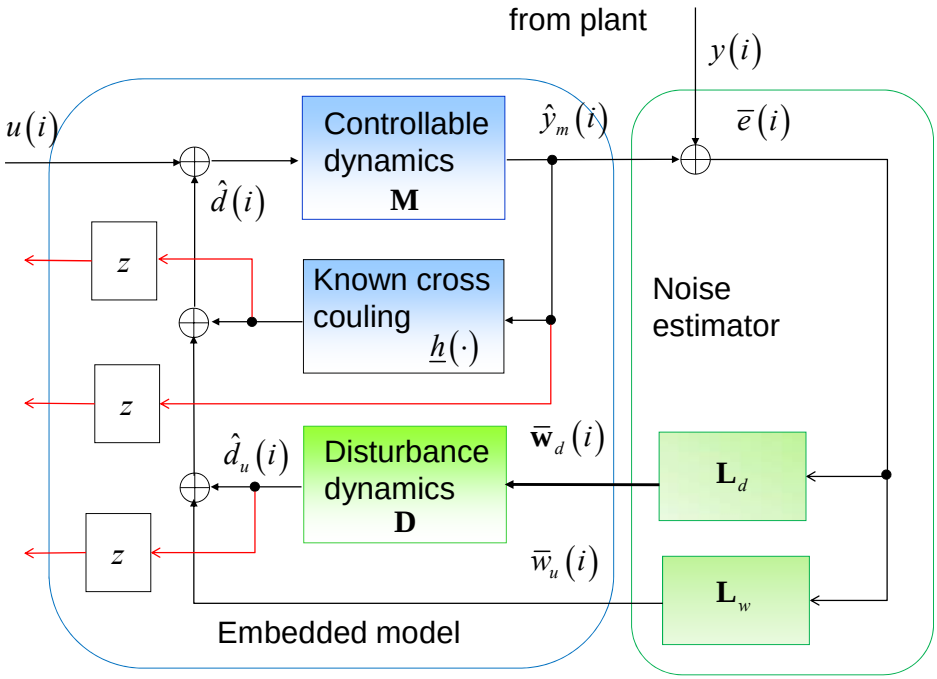

Figure 4 Embedded model and noise estimator.

Figure 4 shows the noise estimator driving the disturbance dynamics. All the output variables of the embedded model are one-step anticipated as indicated by the boxed z.

The coefficients of $\mathbf{L}_d$ and $\mathbf{L}_w$, i.e. the noise estimator gains, are fixed by the state-predictor closed-loop eigenvalues, i.e. by the poles of $\mathbf{S}_m$. The closed-loop spectrum is denoted as

$$\Lambda_m=\{1-\gamma_{m1},...,1-\gamma_{mk},...,1-\gamma_{m\mu}\}, \tag{7}$$

where $\mu\geq n=n_c+n_d$ is the order of the state predictor. Eigenvalues in (20) are written in terms of the complementary eigenvalue γ_{mk}. When the latter is real and $0<\gamma_{mk}\leq 1$, provides the frequency f_{mk} [Hz] through $\gamma_{mk}=\kappa_m 2\pi f_{mk}T$, where $\pi^{-1}\leq\kappa_m\leq 1$ and $\kappa_m\to 1$ as $\gamma_{mk}\to 0$. Asymptotic inequalities in Section 3 will be obtained by assuming equal and real eigenvalues, i.e.

$$\gamma_{mk}=\gamma_m=2\pi f_m T,\ k=1,...,\mu, \tag{7}$$

having set $\kappa_m=1$, i.e. $\gamma_m<<1$. The frequency f_m is referred to as the state-predictor frequency.

The low-frequency asymptote of $\mathbf{S}_m$ follows from (8) and holds

$$\left|\mathbf{S}_{m0}\left(jf\right)\right| = \lim_{f\to 0}\left|\mathbf{S}_{m}\left(jf\right)\right| = \lim_{f\to 0}\left|\left(1+\mathbf{M}\left(\mathbf{D}\mathbf{L}_{d}+\mathbf{L}_{w}\right)\right)^{-1}\right| =$$
$$= \lim_{f\to 0}\frac{1}{1+\left(f_{d0}/f\right)^{d_0}+l_{w0}\left(f_0/f\right)^{m_0}} = \left(\frac{f}{f_{m0}}\right)^{d_0} \quad , \tag{8}$$

where $f_{m0} = f_{d0}$. The high-frequency asymptote of $\mathbf{V}_m$ follows from (6) and holds

$$\lim_{f\to\infty<f_{\max}}\left|\mathbf{V}_{m}\left(jf\right)\right| = \lim_{f\to\infty<f_{\max}}\left|\mathbf{M}\left(\mathbf{D}\mathbf{L}_{d}+\mathbf{L}_{w}\right)\right| = \left(\frac{f_{m\infty}}{f}\right)^{m_\infty} \quad . \tag{9}$$
$$f_{m\infty} = f_{\infty}\left(l_{w\infty}\right)^{1/m_\infty}$$

The frequencies f_{m0} and $f_{m\infty}$ are referred to as the sensitivity and complement bandwidths, and are proportional to f_m through the coefficients κ_{m0} and $\kappa_{m\infty}$ that depend on the spectrum Λ_m in (20). They hold

$$\begin{aligned} f_{m0} &= \kappa_{m0} f_m \\ f_{m\infty} &= \kappa_{m\infty} f_m \\ l_{w0} &= \kappa_{w0} f_m^{n_c} \end{aligned} \quad , \tag{10}$$

where the polynomial relation of l_{w0} in (16) has been added.

2.2.2. Example

Since the noise size $n_w = 3$ is less than the order $n = d_0 = d_\infty = 4$ of the noise-to-output transfer function $\mathbf{MD}$, a dynamic noise estimator is mandatory for stabilizing the closed-loop state predictor (embedded model and noise estimator), as in Canuto, Molano and Massotti (2010). To prove it, assume first a static noise estimator in (15), namely

$$\begin{aligned} \begin{bmatrix} \overline{w}_a \\ \overline{w}_a \end{bmatrix}\left(z\right) &= \begin{bmatrix} l_a \\ l_s \end{bmatrix}\overline{e}\left(z\right) \\ \overline{w}_u\left(z\right) &= l_u \overline{e}\left(z\right) \end{aligned} \quad . \tag{11}$$

The corresponding loop transfer function $\mathbf{MH} = \mathbf{M}\left(\mathbf{D}\mathbf{L}_{d}+\mathbf{L}_{w}\right)$ in (17) is found to be

$$\mathbf{M}\left(z\right)\mathbf{H}\left(z\right) = \frac{l_0\left(z-1\right)^2 + l_1\left(z-1\right)+l_2}{\left(z-1\right)^4} \quad , \tag{12}$$

and the denominator of $\mathbf{S}_m$ in (19) holds

$$\phi_m\left(z\right) = \left(z-1\right)^4 + l_0\left(z-1\right)^2 + l_1\left(z-1\right)+l_2 \quad . \tag{13}$$

Since the polynomial in (27) lacks the third degree coefficient, no gain set $\left\{l_0, l_1, l_2\right\}$ exists capable of stabilizing $\mathbf{S}_m$.

The only alternatives are either to add a fictitious noise on the angular increment $\Delta\theta$ in Figure 3, as it is done by Kalman filters, or to employ a dynamic estimator capable of respecting noise layout and size. As an alternative interpretation of the dynamic estimator, we may think of replacing the missing input noise with a further output q which is linearly independent of $\bar{e}$. In fact, any dynamic filter, in the limit a delay, makes output independent of input. As a result, the number of available feedback channels from model error to noise double, from three to six. It can be shown that stability can only be recovered by tuning the six gains together with the parameters of the dynamic filter from $\bar{e}$ to q.

Assume a first-order filter $q=\left(z-1+\beta\right)^{-1}\bar{e}$, because the noise deficiency is just $n_e=n-n_w=1$. The following noise estimator replaces (25):

$$\begin{aligned}\mathbf{L}_d\left(z\right)&=\begin{bmatrix}l_a\\ l_s\end{bmatrix}+\begin{bmatrix}m_a\\ m_s\end{bmatrix}\left(z-1+\beta\right)^{-1}\\ \mathbf{L}_w\left(z\right)&=l_u+\left(z-1+\beta\right)^{-1}m_u\end{aligned}. \tag{13}$$

The seven gains in (28) must be explicitly related to the closed-loop eigenvalues, or, that is the same, to the poles of $\mathbf{S}_m$, whose cardinality is $\mu=n+n_e=5$. Equal eigenvalues are assumed, namely $\Lambda_m=\left\{1-\gamma_m,...,1-\gamma_m\right\}$. Since the seven gains in (28) satisfy the following five equations

$$\begin{aligned}&\beta=5\gamma_m\\ &l_u=l_{w0}=10\gamma_m^2=\kappa_{w0}f_m^2\\ &l_u\beta+m_u+l_a=10\gamma_m^3\\ &l_a\beta+m_a+l_s=5\gamma_m^4\\ &m_s=\gamma_m^5\end{aligned}, \tag{13}$$

their selection may be optimized. Equation (29) shows that the filter gain β is essential for recovering stability, as already mentioned. Moreover either the pair $\left(m_a,\ m_u\right)$ or $\left(l_a,\ l_s\right)$ can be set to zero. The latter solution, i.e. $l_a=l_s=0$, is preferable, since forcing them to be zero reduces the contribution of $\bar{e}$ which is noisier than q. Using (29) and (24), the asymptote parameters in (22) and (23) become

$$\begin{aligned}&d_0=4,\ f_{m0}=\frac{\left(\beta/m_s\right)^{1/4}}{2\pi T}=\sqrt[4]{5}\,\frac{\gamma_m}{2\pi T}=\kappa_{m0}f_m\\ &m_\infty=2,\ f_{v\infty}=\frac{\sqrt{l_u}}{2\pi T}=\frac{\sqrt{10}\gamma_m}{2\pi T}=\kappa_{m\infty}f_m\end{aligned}. \tag{14}$$

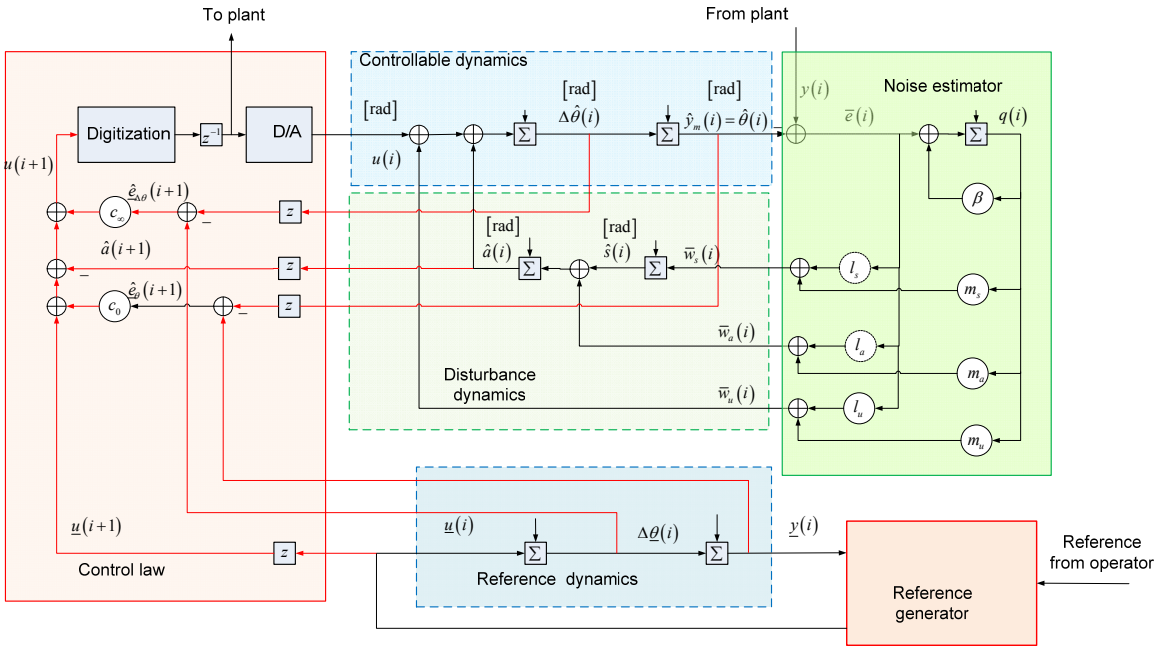

Figure 5 Block diagram of the embedded model plus noise estimator and control law.

Figure 5 shows the block-diagram of the embedded model in Figure 3 plus the dynamic noise estimator (28) and the control law to be outlined in Section 3.1.2. Gains are denoted with circles. Dashed circles correspond to zero gains.

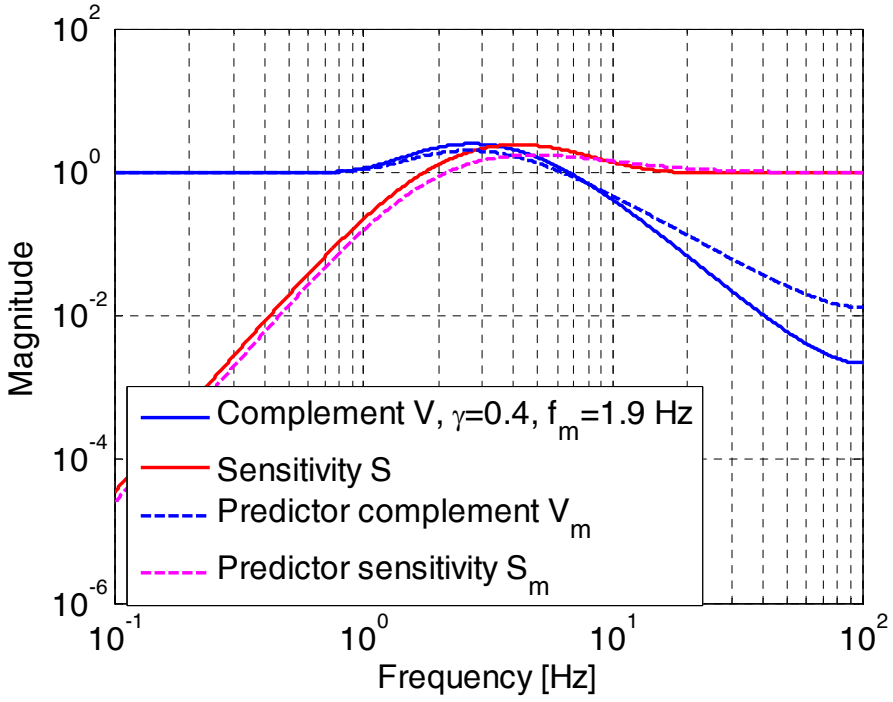

Figure 6 Bode plots (magnitude) of the sensitivity transfer functions and ofits complement.

Figure 6 shows typical Bode plots (magnitude) of the predictor transfer functions (dashed lines), and of the overall transfer functions to be derived in Section 3.

2.3. Reference dynamics and tracking error

Performance refers to a class of reference signals $\underline{y}$ which is assumed to satisfy the same dynamics as in (4), but corrupted by a known disturbance $\underline{d}_u$ as follows

$$\underline{y}(z) = \mathbf{M}(z)\left(\underline{u}(z) + \underline{d}_u(z)\right). \tag{14}$$

Here $\underline{d}_u$ is assumed to be known, which is not the case when it is recorded from measurements. The reference signal class is shaped by the open-loop command $\underline{u}$, which is real-time computed by a reference generator (not treated here, see Figure 5) capable of matching operator requests and technology limits. Typically Model Predictive Control (Camacho and Bordons, 2003) is concerned with it. The reference state is denoted with $\underline{\mathbf{x}}$.

Control performance is assessed by means of the tracking error $\underline{e}_y = \underline{y} - y_m$, satisfying

$$\begin{aligned} \underline{e}_y(z) &= \mathbf{M}(z)\left(\underline{u} + \underline{d}_u - u - d_u - h(\cdot) - w_u - \underline{h}(\cdot)\right)(z) \\ \underline{e}_y(z) &= C_c\left(\underline{\mathbf{x}} - \mathbf{x}_c\right)(z) = C_c\underline{\mathbf{e}}(z) \end{aligned}. \tag{14}$$

In the example, $\underline{d}_u = 0$, and the reference block-diagram is shown in Figure 3, bottom. The reference state vector is denoted by

$$\underline{\mathbf{x}} = \begin{bmatrix} \underline{y} = \underline{\theta} \\ \Delta\underline{\theta} \end{bmatrix}. \tag{15}$$

2.4. Model errors and uncertainties

2.4.1. Generalities

Following the literature (Maciejowski, 1989) two kinds of model errors are treated in addition to innovations $\mathbf{w}_d$ and w_u.

Structured uncertainty is defined by the uncertain 'static' feedback $h(\mathbf{x}_c)$ connecting $\mathbf{x}_c$ to u as in (4). Being unknown, it cannot be explicitly cancelled by the control law in Section 3. The inclusion in (4) of the disturbance d_u allows to surrogate $h(\cdot)$, but at the cost of closed-loop degradation since a feedback link is replaced by a command-independent signal as d_u. Closed-loop stability must be guaranteed. $h(\cdot)$ is assumed differentially bounded. The bound is obtained expanding h around the reference state $\underline{\mathbf{x}}$ as follows

$$\begin{aligned} h(\mathbf{x}_c) &= h(\underline{\mathbf{x}}) + \Delta h(\tilde{\mathbf{x}})(\underline{\mathbf{x}} - \mathbf{x}_c) \\ \tilde{\mathbf{x}} &= \underline{\mathbf{x}} - \alpha(\underline{\mathbf{x}} - \mathbf{x}_c),\ 0 \le \alpha < 1 \end{aligned}. \tag{15}$$

If $\underline{\mathbf{x}}$ and the state tracking error $\underline{\mathbf{e}} = \underline{\mathbf{x}} - \mathbf{x}_c$ are bounded, also $\tilde{\mathbf{x}}$ is bounded. Using (5) and (32), the first order expansion in (34) is written as

$$\Delta h(\tilde{\mathbf{x}})(\underline{\mathbf{x}} - \mathbf{x}_c)(z) = \frac{\Delta h(\tilde{\mathbf{x}})N(z)}{C_c N(z)}\underline{e}(z), \tag{15}$$

and the parametric error $\underline{e}_{\Delta h}$ is defined by

$$\underline{e}_{\Delta h}(z) = \mathbf{M}(z)\,\Delta h(\tilde{\mathbf{x}})(\underline{\mathbf{x}} - \mathbf{x}_c)(z) = \frac{\Delta\mathbf{H}(\tilde{\mathbf{x}}, z)}{\phi(z)}\underline{e}(z), \tag{15}$$

where ϕ has been defined in (5). $\Delta\mathbf{H}(\tilde{\mathbf{x}}, z) = \Delta h(\tilde{\mathbf{x}})N(z)$ is a polynomial having degree $m_h = \deg\Delta\mathbf{H} < \deg\phi$, and bounded coefficients

$$\left|\Delta h_k(\tilde{\mathbf{x}})\right| \le \Delta h_{k,\max}(\underline{\mathbf{x}}),\ k = 0..., m_h - 1. \tag{15}$$

The same polynomial having the bounds in (37) as coefficients is denoted with $\Delta\mathbf{H}_{\max}(\underline{\mathbf{x}}, z)$.
Unstructured uncertainty is defined as an uncertain dynamic operator $\partial\mathbf{P}(y_m, ...)$ from the model output y_m to the plant output y. Input-output stability and linear, time-invariance are assumed, implying that the model error (1) has the expression

$$e(z) = \partial\mathbf{P}(z;\mathbf{p})\,y_m(z) + w_y(z),\ \partial\mathbf{P}(z;\mathbf{p}) \in \partial\mathcal{P}, \tag{15}$$

where $\partial\mathcal{P}$ is the uncertainty class defined by a parameter vector $\mathbf{p} \in \Pi$ belonging to a bounded set Π, and w_y is the measurement noise. The transfer function $\partial\mathbf{P}$ results from the sampled-data transform of a continuous-time dynamics enclosed between the plant zero-order hold and the output sampler. Since $\partial\mathbf{P}$ is dropped from the embedded model, it may affect the overall stability, and calls for robust stability conditions. Here we assume that there exists a worst-case element $\partial\mathbf{P}_{\max}(z;\mathbf{p}_{\max})$ in $\partial\mathcal{P}$ such that

$$\begin{aligned} &\max_{f<f_{\max}}\left|\partial\mathbf{P}_{\max}(f)\right| = \max_{\partial\mathcal{P}}\max_{f<f_{\max}}\left|\partial\mathbf{P}(f)\right| \\ &0 < \arg\max_{f<f_{\max}}\left|\partial\mathbf{P}_{\max}(f)\right| = f_{\partial\mathbf{P}} = \min_{\partial\mathcal{P}}\arg\max_{f<f_{\max}}\left|\partial\mathbf{P}(f)\right| < f_{\max} \end{aligned}, \tag{15}$$

i.e. the peak of the worst case is the highest peak in the class $\partial\mathcal{P}$, and the peak frequency $f_{\partial\mathbf{P}}$ is the lowest in the class $\partial\mathcal{P}$.

2.4.2. Example

Using (9), the transfer function in (36) is found to be

$$\frac{\Delta H(\tilde{\mathbf{x}}, z)}{\phi(z)} = \frac{\Delta h_1(\Delta\tilde{\theta})(z-1) + \Delta h_0(\tilde{\theta})}{(z-1)^2},\ m_h = 1,\ n_c = 2, \tag{15}$$

where the bounds of the dimensionless coefficients in (40) are given in terms of the frequencies f_g and $f_{\Delta\theta}(\underline{\Delta\theta})$, i.e.

$$\begin{aligned} &\left|\Delta h_1(\Delta\tilde{\theta})\right| = \mathrm{sgn}(\Delta\theta)\,dA(|\Delta\theta|)/d|\Delta\theta|\Big|_{\Delta\theta=\Delta\tilde{\theta}} T/J \le 2\pi f_v(\underline{\Delta\theta})T \\ &\left|\Delta h_0(\tilde{\theta})\right| = mglT^2\left|\sin(\tilde{\theta})\right|/J \le (2\pi f_g T)^2 \end{aligned}. \tag{15}$$

The frequency square in (41) is imposed by $n_c = \deg\phi = 2$. f_g is the 'pendulum' natural frequency of the arm, whereas $2\pi f_{\Delta\theta}(\underline{\Delta\theta})$ is the friction/inertia pole, depending on the reference angular rate $\underline{\Delta\theta}$, and such that $f_{\Delta\theta}(\underline{\Delta\theta}) \le f_{\Delta\theta}(0)$.

Neglected dynamics is restricted to gear backlash and torsional deformation. Due to backlash, dynamics is nonlinear. It can be linearly approximated for $|e| \geq e_{\min}$, the lower bound corresponding to the backlash width. Then

$$\begin{aligned} &\partial\mathbf{P}(z) \simeq -(z-1)^2\left((z-1)^2 + \beta_t(z-1) + \alpha_t\right)^{-1} \\ &\alpha_t \simeq (2\pi f_t T)^2,\ \beta_t \simeq \alpha_t(\alpha_t + 2\zeta_t),\ \mathbf{p}^T = [f_t \quad \zeta_t] \in \Pi \end{aligned}, \tag{15}$$

expresses the fractional error between the motor-gear-arm dynamics having flexible transmission and the rigid body (9). The parameters in $\mathbf{p}$ are the uncertain natural frequency f_t and the damping coefficient ζ_t. Typical Bode diagrams, including a ball and beam device, are in Canuto, Acuna-Bravo, Molano and Perez (2012). The response peak and the peak frequency in (39) hold

$$f_{\partial\mathbf{P}} = f_{t,\min} = \min_{f_t \in \Pi} f_t,\ \max_{\mathbf{p}\in\Pi} \partial\mathbf{P}_{\max}(z) = \left(2\zeta_{t,\min}\right)^{-1}. \tag{15}$$

3. Control law and the error loop

3.1. Control law and tracking error

3.1.1. Generalities

Given (4) and (31), in order to respect causality, the control law must depend either on the state variables or on their combinations like y_m and d_u, but not on w_u. In addition, it must guarantee that the tracking error $\underline{e}_y = \underline{y} - y_m$ is bounded, and that the mean value tends asymptotically to zero. The control law

$$u(z) - \underline{u}(z) - \underline{d}_u(z) = \mathbf{C}(z)\left(\underline{e}(z) + \hat{e}(z)\right) - d_u(z) - h(\mathbf{x}_c) + \hat{e}_d(z) \tag{15}$$

can be shown to bound $\underline{e}_y$ under appropriate conditions on $\mathbf{C}$, and on the prediction errors $\hat{e}_y$ and $\hat{e}_d$. In (44), $\mathbf{C}(z)$ is usually improper with a bounded low-frequency gain $c_0 = \lim_{z\to 1}\mathbf{C}(z) \neq 0$ and

$$\lim_{f\to\infty<f_{\max}} |\mathbf{C}(jf)| = c_\infty f^{m_\infty - 1}. \tag{16}$$

Inserting (44) into (32), simple manipulations yield

$$\left(I + \mathbf{M}(z)\mathbf{C}(z)\right)\underline{e}_y(z) = -\mathbf{M}(z)\mathbf{C}(z)\hat{e}_y(z) - \mathbf{M}(z)\left(\hat{e}_d + \overline{e}_w\right)(z) - \mathbf{M}(z)\overline{w}_u(z). \tag{17}$$

Then, by replacing (13) in (46), the tracking error equation follows

$$\underline{e}_y(z) = -\hat{e}_y(z) - \mathbf{S}_c(z)\mathbf{M}(z)\overline{w}_u(z). \tag{17}$$

In (47) the control sensitivity $\mathbf{S}_c = (1 + \mathbf{MC})^{-1}$ makes its appearance, and the sign of $\hat{e}_y$ is due to a different sign of y_m in the errors. The asymptotes of $\mathbf{S}_c\mathbf{M}$ and $\mathbf{V}_c = 1 - \mathbf{S}_c$ can be found to be

$$\begin{aligned} &\lim_{f\to 0}|\mathbf{S}_c(jf)\mathbf{M}(jf)| = \lim_{f\to 0}\left|(1+\mathbf{MC})^{-1}\mathbf{M}\right| = \lim_{f\to 0}\frac{(f_0/f)^{m_0}}{1+(f_0/f)^{m_0}c_0} = \frac{1}{c_0} \\ &|\mathbf{V}_{c\infty}(jf)| = \lim_{f\to\infty<f_{\max}}|\mathbf{V}_c(jf)| = \lim_{f\to\infty<f_{\max}}|\mathbf{MC}| = \frac{c_\infty(f_\infty)^{m_\infty}}{f} = \frac{f_{c\infty}}{f} \end{aligned}. \tag{18}$$

The coefficients of $\mathbf{C}$ derive from the poles of $\mathbf{S}_c$, of the order $\kappa = n_c \geq m_\infty$, and are designed to stabilize $\mathbf{S}_c$. Likewise in (20), the closed-loop spectrum is denoted with

$$\Lambda_c = \{1-\gamma_{c1},...,1-\gamma_{ck},...,1-\gamma_{c\kappa}\}, \tag{18}$$

and equal eigenvalues are assumed, $\gamma_{ck} = \gamma_c = 2\pi f_c T$. $k = 1,...,\kappa$. The control-law frequency is f_c. Similar to (24) we can write

$$\begin{aligned} f_{c\infty} &= \kappa_{c\infty} f_c \\ c_0 &= \kappa_{c0} f_c^{n_c} \end{aligned} \tag{19}$$

Equation (47) may be better understood if one restricts to a pair of ideal conditions.

1) Model-based control law: it corresponds to $\hat{e}_d = 0$ and $\bar{e}_w = 0$, and to $\hat{e}_y = 0$ in (13), and to the ideal equality

$$\underline{e}_y = -\mathbf{S}_c \mathbf{M} w_u . \tag{20}$$

in (47). Performance only depends on the non-rejected noise w_u and initial conditions.

2) Anti-causal law: it corresponds to include $\bar{w}_u$ in (44), which simplifies (47) to the ideal equality

$$\underline{e}_y = -\hat{e}_y . \tag{21}$$

Moreover, adding $\hat{e}_d = 0$ and $\bar{e}_w = 0$ (model-based assumptions), tracking error becomes zero, less the free-response. Anti-causal laws cannot be realized since $u(i)$ depends on $y(i-1)$, whereas $\bar{w}_u(i)$ depends on $y(i)$. In terms of transfer functions, it would mean $\mathbf{S}_c \to 0$ for $f < f_{\max}$ (the open switch in Figure 2 below $\mathbf{S}_c\mathbf{M}\mathbf{L}_w$), which is unrealizable because of the Bode's integral theorem (Maciejowski, 1989, and Wu and Jonckheere, 1992).

Clearly (47) is a combination of the ideal equalities (51) and (52).

Figure 7 shows the whole control unit that is built around the embedded model: the control law interfaces model an plant, the noise estimator interfaces plant and model, and the reference generator interfaces operator/plant and model. The delay z^{-1}, from control law to plant, balances the model one-step predictions. Digitization converts the computed command to a digital signal, and may include a nonlinear inversion. The opposite is denoted with D/A and provides the embedded model with the same command dispatched to the plant.

The final expression relating $\underline{e}_y$ to the model error e and to the output disturbance d_y in (4) is obtained as follows. Firstly, by replacing (15) and (18) in (47) one finds

$$\underline{e}_y = -\left(I + \mathbf{S}_c \mathbf{M} \mathbf{L}_w\right) \hat{e}_y - \mathbf{S}_c \mathbf{M} \mathbf{L}_w e . \tag{22}$$

Then, by replacing the prediction error $\hat{e}_y$ through (19) and by defining the overall 'control sensitivity' $\mathbf{S}$ and the complement $\mathbf{V} = 1 - \mathbf{S}$ as follows

$$\begin{aligned} \mathbf{S} &= \mathbf{S}_m + \mathbf{S}_w \\ \mathbf{V} &= 1 - \mathbf{S} = \mathbf{V}_m - \mathbf{S}_w , \\ \mathbf{S}_w &= \mathbf{S}_c \mathbf{M} \mathbf{L}_w \mathbf{S}_m \end{aligned} \tag{23}$$

the final expression is obtained

$$\underline{e}(z) = \mathbf{V}(z)e(z) - \mathbf{S}(z)d_y(z). \tag{23}$$

The following alternative expression of $\mathbf{V}$ will be employed hereafter:

$$\mathbf{V} = \mathbf{V}_m - \mathbf{S}_c\mathbf{M}\mathbf{L}_w\mathbf{S}_m = \mathbf{V}_m - \mathbf{S}_c\mathbf{M}(\mathbf{H} - \mathbf{D}\mathbf{L}_d)\mathbf{S}_m = \mathbf{V}_m\mathbf{V}_c + \mathbf{S}_c\mathbf{M}\mathbf{D}\mathbf{L}_d\mathbf{S}_m. \tag{24}$$

The high-frequency asymptotes of the two terms in (56) descend from (8), (23) and (48), and hold

$$\begin{aligned} &\lim_{f\to\infty<f_{\max}} |\mathbf{V}_m\mathbf{V}_c| = \frac{(f_{m\infty})^{m_\infty} f_{c\infty}}{f^{m_\infty+1}} = \left(\frac{f_{v\infty}}{f}\right)^{m_\infty+1} \\ &\lim_{f\to\infty<f_{\max}} |\mathbf{S}_c\mathbf{M}\mathbf{D}\mathbf{L}_d\mathbf{S}_m| = (f_{d\infty}/f)^{d_\infty} \end{aligned}. \tag{25}$$

Thus, if $d_\infty > m_\infty + 1$ and $f_{v\infty} \geq f_{d\infty}$, the former asymptote in (57) dominates and the asymptote simplifies to

$$\begin{aligned} &|\mathbf{V}_\infty| = \lim_{f\to\infty<f_{\max}} |\mathbf{V}(jf)| = \left(\frac{f_{v\infty}}{f}\right)^{m_\infty+1}, f \geq f_{v\infty} \\ &f_{v\infty} = \kappa_{v\infty} f_m / \gamma^{1/(m_\infty+1)},\ \kappa_{v\infty} = \kappa_{m\infty}\kappa_{c\infty}^{1/(m_\infty+1)} \end{aligned}. \tag{26}$$

The overall functions $\mathbf{S}$ and $\mathbf{V}$ combine the predictor transfer functions $\mathbf{S}_m$ and $\mathbf{V}_m$ with the causality correction $\mathbf{S}_w$. The latter is imposed by w_u not being rejected. Equation (55) is the basic 'error loop' equation, to be further elaborated by making explicit e and d_y.

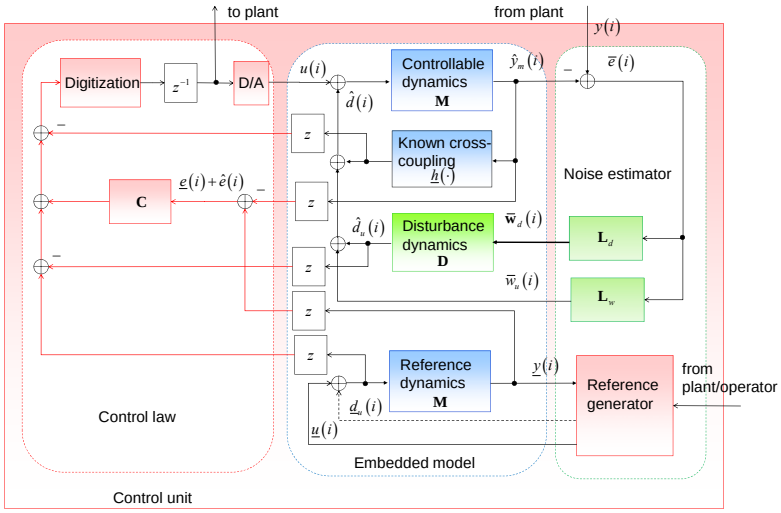

Figure 7 The control unit built around the embedded model.

3.1.2. Example

$\mathbf{C}$ is a proportional plus derivative compensator, i.e.

$$\mathbf{C}(z) = c_\infty(z-1) + c_0. \tag{26}$$

Assuming that the poles of $\mathbf{S}_c$ are equal and collected in $\Lambda_c = \{1-\gamma_c, 1-\gamma_c\}$, the gain equations are $c_\infty = 2\gamma_c$, $c_0 = \gamma_c^2 = \kappa_{c0} f_c^2$. The overall block diagram of the control unit is in Figure 5. The errors

$$\begin{aligned} \hat{\underline{e}}_\theta(i) &= \underline{e}_\theta(i) + \hat{e}_\theta(i) \\ \hat{\underline{e}}_{\Delta\theta}(i) &= \underline{e}_{\Delta\theta}(i) + \hat{e}_{\Delta\theta}(i) \end{aligned} \tag{27}$$

are the 'measured' tracking errors already defined in (3).

3.2. Stability and performance versus structured and unstructured uncertainty

3.2.1. Robust stability

Input-output stability of (55) occurs if and only if

1) $\mathbf{S}$ is asymptotically stable, which in turn requires the stability of $\mathbf{S}_m$ and $\mathbf{S}_c$, and
2) the input signals e and d_y are bounded and causally independent of $\underline{e}_y$.

The latter condition only occurs when structured and unstructured uncertainties are zero: $h = \partial\mathbf{P} = 0$ (the open switches in Figure 2), i.e.

$$\begin{aligned} e(z) &= w_y(z) \\ d_y(z) &= \mathbf{M}(z)\left(\mathbf{D}(z)\mathbf{w}_d(z) + w_u(z)\right) \end{aligned}, \tag{27}$$

and imply that the tracking error is only forced by an 'unpredictable' noise as in the Linear Quadratic Gaussian control (Kwakernaak and Sivan, 1972).

On the contrary, making explicit structured and unstructured uncertainties in (55) by means of (38) and (4), and dropping z, the implicit 'error loop' equation follows:

$$\underline{e}_y = \mathbf{V}\partial\mathbf{P}\left(\underline{y} - \underline{e}_y\right) - \mathbf{SM}h(\mathbf{x}_c) + \mathbf{V}w_y - \mathbf{SM}\left(\mathbf{D}\mathbf{w}_d + w_u\right). \tag{27}$$

Equation (62) is made explicit in $\underline{e}_y$ through (34) and (36), which yields the stability equation

$$\left(1 + \mathbf{V}\partial\mathbf{P} + \mathbf{S}\Delta\mathbf{H}(\tilde{\mathbf{x}})/\phi\right)\underline{e}_y = \mathbf{V}\left(\partial\mathbf{P}\underline{y} + w_y\right) - \mathbf{SM}\left(h(\underline{\mathbf{x}}) + \mathbf{D}\mathbf{w}_d + w_u\right). \tag{27}$$

Equation (62) is graphically represented in Figure 2. There, the uncertainties in Figure 1 and the control unit are combined so as to build the 'error loop'. The control unit, detailed in Figure 7, has been transformed by the above derivation into a combination of the ingredients of $\mathbf{S}$ and $\mathbf{V}$, namely, $\mathbf{M}$ (controllable dynamics), $\mathbf{S}_m$ (state predictor), $\mathbf{S}_c$ (control law and controllable dynamics) and $\mathbf{L}_w$ (noise estimator of w_u).

Observe that

1) the unstructured uncertainty $\partial\mathbf{P}$ is filtered by $\mathbf{V}$, which being a low-pass filter, implies that $\partial\mathbf{P}$ should become significant only at higher frequencies;
2) the structured uncertainty $\Delta\mathbf{H}$ is filtered by $\mathbf{S}$, which being a high-pass filter, implies that $\Delta\mathbf{H}$ should become significant only at lower frequencies;

A sufficient stability condition in terms of the frequency response may descend from the 'small-gain theorem' in Desoer and Vidyasagar (1975), and leads to

$$\max_{|f|<f_{\max}} \left|\mathbf{V}(f)\partial\mathbf{P}(f) + \mathbf{S}(f)\Delta\mathbf{H}(\tilde{\mathbf{x}}, f)/\phi(f)\right| \le \eta < 1, \tag{27}$$

where η^{-1} is a stability margin. Inequality (64), which is the key result, is similar but not equal to inequalities in Doyle, Francis and Tannenbaum (1992), where stability and performance inequalities are combined.

3.2.2. Performance

Inequality (64) allows to rewrite (63) as

$$\left|\underline{e}_y\right| \le \left(1-\eta\right)^{-1}\left|\mathbf{V}\left(\partial\mathbf{P}\underline{y}+w_y\right)-\mathbf{SM}\left(h\left(\underline{\mathbf{x}}\right)+\mathbf{D}\mathbf{w}_d+w_u\right)\right|, \tag{27}$$

which becomes the performance inequality, $|\cdot|$ being a suitable norm. It is out of the paper aim to discuss and apply (65). It suffices to point out that it can be split in two components:

1) the deterministic term $\mathbf{V}\partial\mathbf{P}\underline{y}-\mathbf{SM}h\left(\underline{\mathbf{x}}\right)$ depending on the reference trajectory,
2) the 'random' term $\mathbf{V}w_y-\mathbf{SM}\left(\mathbf{D}\mathbf{w}_d+w_u\right)$ depending on noise components.

Given η and the eigenvalue range derived from (64) in Section 3.3, the first term in (65) fixes the slew rate of the reference trajectory, whereas the random part fixes sensor and actuator noise. It has been already remarked that $\underline{e}_y$ is only available through simulated runs, and is related to the measured control error e_y - defined as reference minus measure - through the model error e as in (3). Therefore, if the tracking error $\underline{e}_y$ is made bounded by (65) and $\left|\underline{e}_y\right| << |e|$ - which are mandatory requirements - the control error e_y becomes the opposite of the model error e. Alternative and measurable conditions derive from the former decomposition of e_y in (3). In the case that $\left|\hat{\underline{e}}_y\right| \to 0$, which corresponds to approach the anti-causal law (52), the control error becomes the opposite of the measured model error $\overline{e}$, a condition that can be easily verified.

3.3. Asymptotic stability inequalities

Explicit expressions of (64) and (65) are obtained under the following assumptions.

1) State predictor and control law have uniform but distinct eigenvalues as already stated in (21) and (49). Their ratio

$$\gamma = \gamma_m / \gamma_c = f_m / f_c \tag{27}$$

   is referred to as the control frequency ratio.

2) The components of the inequality (64) reach their maximum values within separate frequency domains: the sensitivity frequency band, $f \le f_{s0}$, and the complementary sensitivity band, $f \ge f_{v\infty}$, to be defined below.

Consider the former component in (64) due to parametric uncertainty, and replace $\mathbf{S}\left(f\right)$ with the low-frequency asymptote $\mathbf{S}_0\left(f\right)$. The latter, derived from (22), (48) and (24), holds

$$\begin{aligned} &\left|\mathbf{S}_0\left(jf\right)\right| = \lim_{f\to 0}\left|\mathbf{S}\left(jf\right)\right| = \operatorname{im}_{f\to 0}\left|\mathbf{S}_m\left(1+\mathbf{S}_c\mathbf{M}\mathbf{L}_w\right)\right| = \left(f/f_{s0}\right)^{d_0},\ f \le f_{s0} \\ &f_{s0} = f_{m0}/\left(1+l_{w0}/c_0\right)^{1/d_0} = \kappa_{m0}f_m/\left(1+\kappa_s\gamma^{n_c}\right)^{1/d_0} < f_{m0} \end{aligned}, \tag{27}$$

where $\kappa_s = \kappa_{w0}/\kappa_{c0}$. Equation (67) affirms that the overall sensitivity BW f_{s0} is narrower than the state predictor f_{m0}, because $\mathbf{S}_c$ is not zero. Since, as stated in Section 2.4, $\Delta\mathbf{H}\left(\tilde{\mathbf{x}}\right)/\phi$ is strictly proper and $n_c = \deg\phi < d_0$, the parametric component $\mathbf{S}\Delta\mathbf{H}/\phi$ in (64) achieves its maximum close to f_{s0}. Then, replacing the coefficients of $\Delta\mathbf{H}\left(\tilde{\mathbf{x}}\right)$ with their bound in (37), the following inequality results

$$\max_{|f|<f_{\max}} \left|\mathbf{S}_0(f)\Delta\mathbf{H}(\tilde{\mathbf{x}},f)/\phi(f)\right| \le (1+\varepsilon_s)\left|\Delta\mathbf{H}_{\max}(\underline{\mathbf{x}},f_{s0})/\phi(f_{s0})\right|, \tag{27}$$

where $\varepsilon_s << 1$ accounts for the actual $|\mathbf{S}(f)|$ in the neighbourhood of f_{s0}.

Maximization of the second component employs the asymptote (58). Considering (39) and assuming $f_{\partial\mathbf{P}} \ge f_{v\infty}$, a local maximum of $|\mathbf{V}_\infty(f)\partial\mathbf{P}(f)|$ occurs for $f_{v\infty} \le f \le f_{\partial\mathbf{P}}$, since $|\mathbf{V}_\infty(f)|$ in (58) is monotonically decreasing. Having the Example in mind (Section2.1.2 and following), we assume

$$\max_{|f|<f_{\max}} \left|\mathbf{V}(f)\partial\mathbf{P}(f)\right| \le (1+\varepsilon_v)\left(f_{v\infty}/f_{\partial\mathbf{P}}\right)^{v_\infty}\left|\partial\mathbf{P}_{\max}(f_{\partial\mathbf{P}};\mathbf{p}_{\max})\right|, \tag{27}$$

where $\varepsilon_v < 1$ plays the role of ε_s in (68).

Finally, (64) splits into the asymptotic inequalities

$$\begin{aligned} &f_{v\infty} \le f_{\partial\mathbf{P}}\left(\eta/\left|\partial\mathbf{P}_{\max}(f_{\partial\mathbf{P}};\mathbf{p}_{\max})\right|\right)^{1/v_\infty},\ \eta<1 \\ &\left|\phi(f_{s0})\right| \ge \left|\Delta\mathbf{H}_{\max}(\underline{\mathbf{x}},f_{s0})\right|/\eta,\ \eta<1 \end{aligned}, \tag{27}$$

where ε_s in (68) and ε_v in (69) have been absorbed by the stability margin $1/\eta$.

Given η, (70) can be solved for $f_{v\infty} < f_{\max}$ and $f_{s0} < f_{\max}$. The first inequality in (70) provides an upper bound to $f_{v\infty}$. The second is a polynomial inequality, that, since $\deg\phi > \deg\Delta\mathbf{H}_{\max}(\cdot)$, provides a lower bound as $f_{s0} \to \infty$. Bounds in (70), if feasible, can be transformed into bounds on the state-predictor frequency f_m, and on the control ratio γ in (66), by replacing the expressions (67) and (58) of f_{s0} and $f_{v\infty}$, respectively. At the end, (70) can be replaced by

$$f_{m,\min}(\gamma,\eta) \le f_m \le f_{m,\max}(\gamma,\eta) < f_{\max}. \tag{27}$$

Inequality (71) proves the following.

1) A robust design is driven by the predictor frequency f_m, which is bounded from above by the neglected dynamics and bounded from below by the parametric uncertainty.
2) The admissible band $\Delta f_m = f_{m,\max}/f_{m,\min} \ge 1$ depends on the control ratio $\gamma > 0$ and on the stability margin $\eta^{-1} > 1$. The asymptotic approximations that have been adopted to obtain (71), tend to be accurate for $\gamma \le 1$.

Because of the assumptions made at the beginning of this section, the closed-loop eigenvalues entailed by (71) must be kept as first trial, to be refined by simulation and in-field. The admissible band $\Delta f_m(\gamma) \ge 1$ provides degrees-of-freedom to the performance inequality (65) as in Canuto (2004, 2008).

3.4. Example: robust stability design

Using (9), (28) and (59), the low-frequency asymptote of **S** and the high-frequency asymptote of **V** can be written as

$$\begin{aligned} &\mathbf{S}_0(z) = (z-1)^4\,\beta(1+l_u/c_0)/m_s \\ &\mathbf{V}_\infty(z) = (z-1)^{-3}\,l_u c_\infty \end{aligned}. \tag{27}$$

They correspond to the asymptotes of the Bode plots in Figure 6. Expressing f_{s0} and $f_{v\infty}$ in terms of f_m and γ as in (67) and (58), yields

$$\begin{aligned} f_{s0}\left(f_m,\gamma\right) &= f_m / \left(5\left(1+2\gamma^2\right)\right)^{1/4} \\ f_{v\infty}\left(f_m,\gamma\right) &= f_m \left(20/\gamma\right)^{1/3} \end{aligned} . \tag{27}$$

The stability inequalities in (70) become

$$\begin{aligned} f_{s0}^2\left(f_m,\gamma\right) - \frac{f_v\left(\underline{\Delta\theta}\right)}{\eta} f_{s0} &\geq \frac{f_g^2}{\eta} \\ f_{v_\infty}\left(f_m,\gamma\right) &\leq f_{t,\min}\left(2\eta\zeta_{t,\min}\right)^{1/3} \end{aligned} . \tag{27}$$

They have been solved for f_m and γ in the Table I using the parameters of the same Table.

TABLE I PARAMETERS AND DESIGN

Parameter	Symbol	Unit	Value	Comments
Gravity frequency	f_g	Hz	0.11	
Friction frequency	f_v	Hz	0.25	$\lvert\underline{\Delta\theta}\rvert \geq 0.75$ mrad
Transmission frequency	$f_{t,\min}$	Hz	22	
Damping	$\zeta_{t,\min}$		0.025	
Backlash	$e_{\min}$	mrad	≤0.4	
Predictor frequency: case 1	$f_{m,\max}$	Hz	2.2	@ $\eta = 0.5$, $\gamma = 1$
idem, case 2	$f_{m,\max}$	Hz	2.6	@ $\eta = 0.5$, $\gamma = 0.4$
idem, case 3	$f_{m,\max}$	Hz	1.3	@ $\eta = 0.5$, $\gamma = 0.2$

Three alternative eigenvalues, denoted as case 1, 2 and 3, have been selected: they correspond to the square marks on the line $f_{m,\max}\left(\gamma\right)$ in Figure 8 and to $\gamma = \{1, 0.4, 0.2\}$. As shown by Figure 9, $\gamma = 1$ corresponds to the widest admissible band Δf_m, whereas $\gamma = 0.2$ is a lower threshold since uncertainty cannot be more accommodated for $\gamma < 0.2$. In practice, given the state predictor frequency f_m, the control law frequencies f_c and $f_{v\infty}$ in (73) become too wide, and the first inequality in (70) (accommodating the neglected dynamics) cannot be guaranteed.

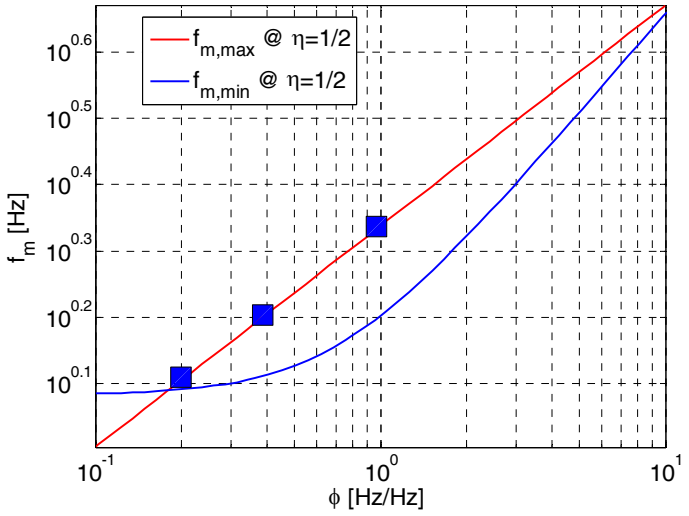

Figure 8 Admissible state predictor frequency f_m for $\eta = 0.5$.

The design has been restricted to the upper bound $f_{m,\max}(\gamma)$ and to the eigenvalue region $\gamma \le 1$ in order to force the control error e_y to stay within the target bounds in Figure 10. The frequency bounds $f_{m,\max}$ and $f_{m,\min}$ are shown in Figure 8 versus the eigenvalue ratio γ for a stability margin $\eta^{-1} = 2$. The margin is sufficient since the worst-case uncertainties enter the bound expressions (74).

Figure 9 shows the admissible frequency band Δf_m. The horizontal dashed line corresponds to $\Delta f_m = 1$ (the band has no width). The largest achievable stability margin is close to 4. The widest admissible band occur for $\gamma \cong 1$.

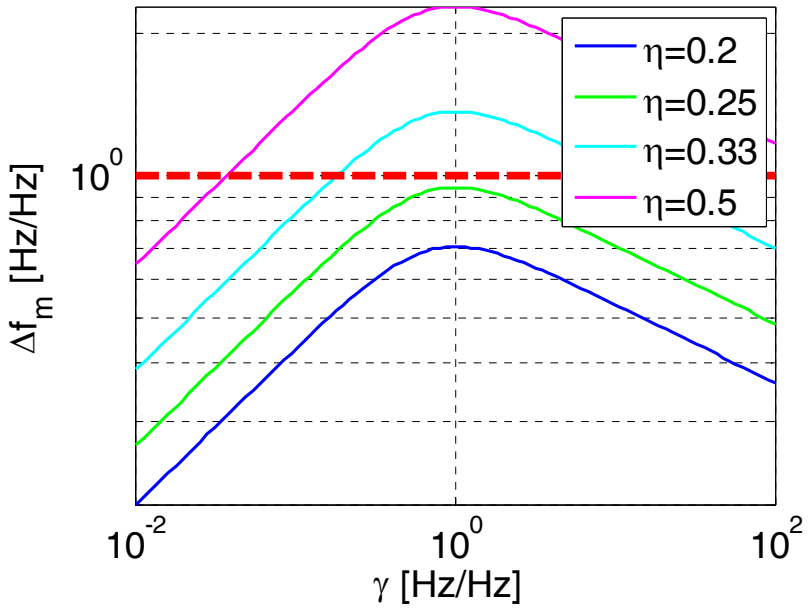

Figure 9 The admissible frequency band Δf_m versus γ and η.

4. Simulated and experimental results

The alternative designs in Table I has been tested through simulation and a ball and beam device leaving the ball uncontrolled. Their performance have been compared through the control error e_y. Angular position is measured with an incremental encoder on the gear output shaft. Encoder quantization is of the same order of the backlash in Table I. Up and down motion is driven by a suitable reference generator thataccounts for speed and current limits, which impose motion duration. Figure 10 shows the control error during up and down motion and intermediate halt intervals. Bounds to control error have been set larger during motion (dashed lines in Figure 10).

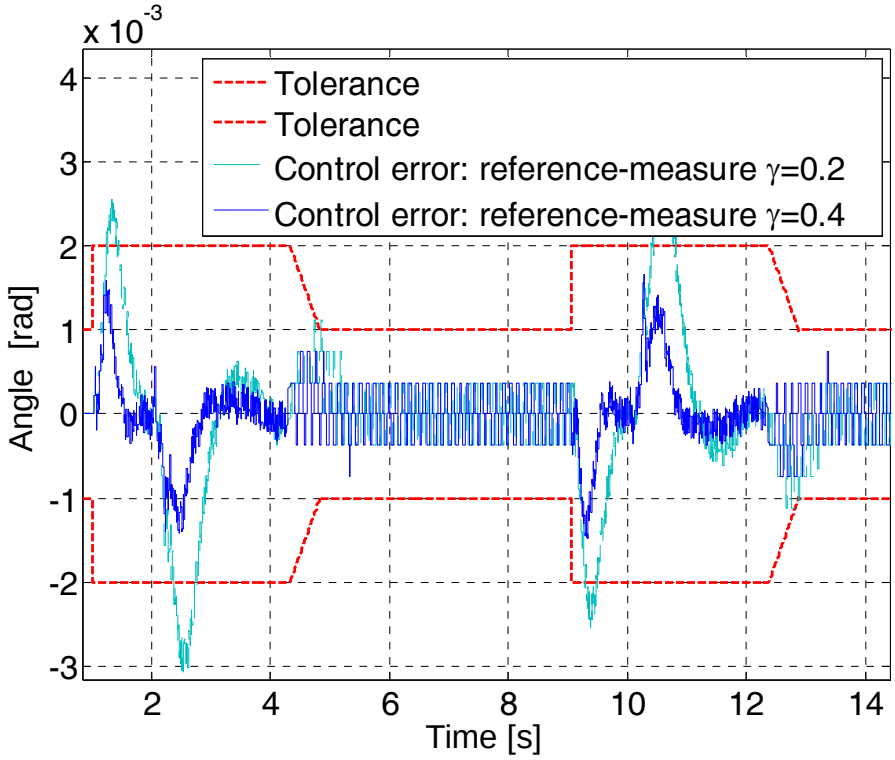

Figure 10 Simulated control error for two different designs.

Performance improves by increasing γ from 0.2 (case 3) to 0.4 (case 2) and to 1 (case 1), as Figure 10 shows. That is reasonable since a lower γ in Figure 8 narrows the predictor BW and consequently increases the norm of the second term in the right-hand side of (65). This clearly occurs during motion, say from 9 s to 12 s in Figure 10, when friction, assumed unknown, cannot be fully cancelled by the predicted $\hat{d}_u$ in (44). When the set-point is reached, control error is dominated by backlash and no significant difference appears. The case 1, not shown in Figure 10, behaves more or less as the case 2, except that the control error becomes more noisy, due to a larger control BW. Therefore, case 2 looks a good trade-off: the relevant transfer functions have been reported in Figure 6.

Figure 11 shows the achievement of a set point for the cases 2 and 3. One may observe that the case 3 is much slower in the set point achievement, as anticipated above. The backlash effect cannot be cancelled, being smaller than the encoder quantization. It couples with sensor quantization and gives rise to a limit cycle around the set point not larger than 1 bit.

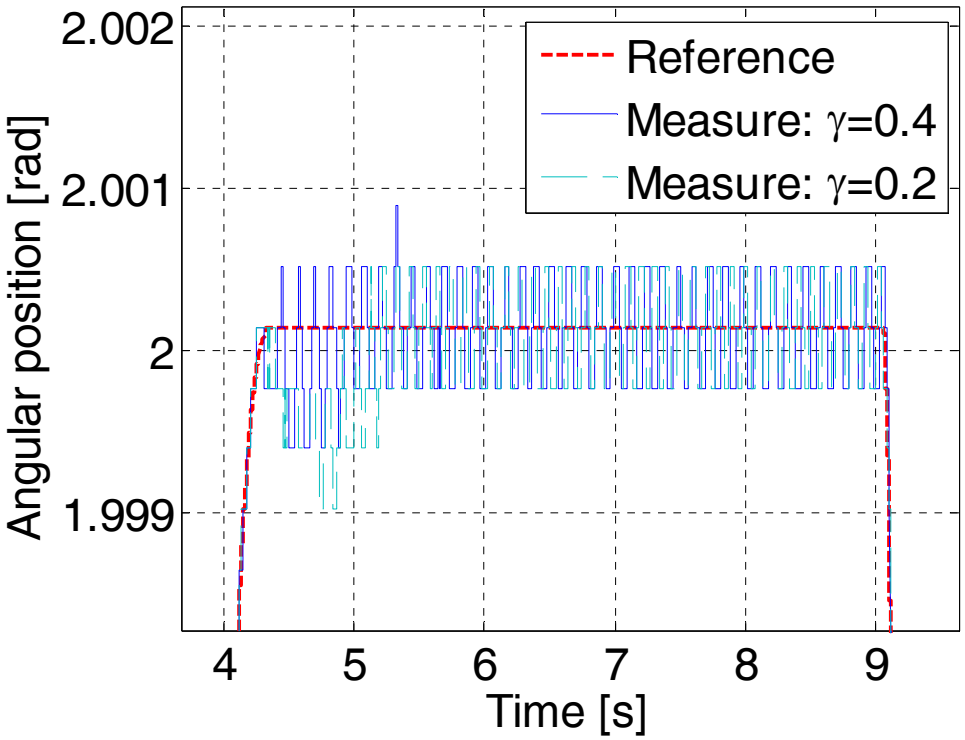

Figure 11 Set point achievement for two different designs.

The trapezoidal angular position of the gear pivoting the beam is measured by the gear encoder and is shown in Figure 12. The difference between reference and measured angle - the control error - can be perceived from the enlargement in Figure 13, when the reference angle reaches the maximum value. The measured position reaches the maximum value after a damped oscillation ending in a limit cycle (the square wave overlapping the constant reference) imposed by backlash, friction and encoder quantization. Figure 12 shows the ball stroke (both simulated and experimental), that, being uncontrolled, swings between the beam extremes with some delay owing to friction.

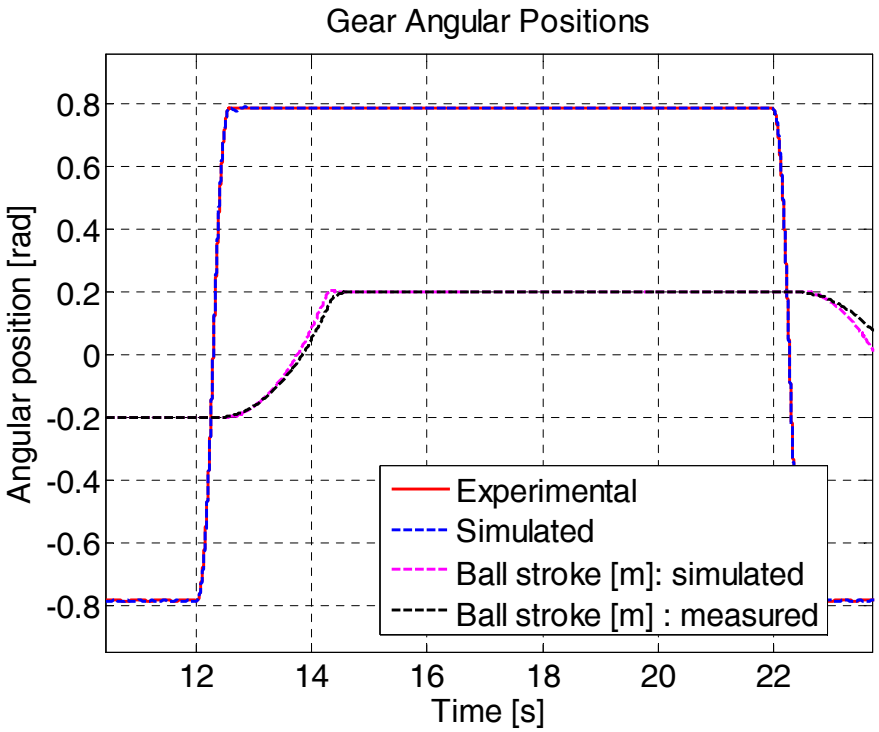

Figure 12 Experimental and simulated gear and ball motion.

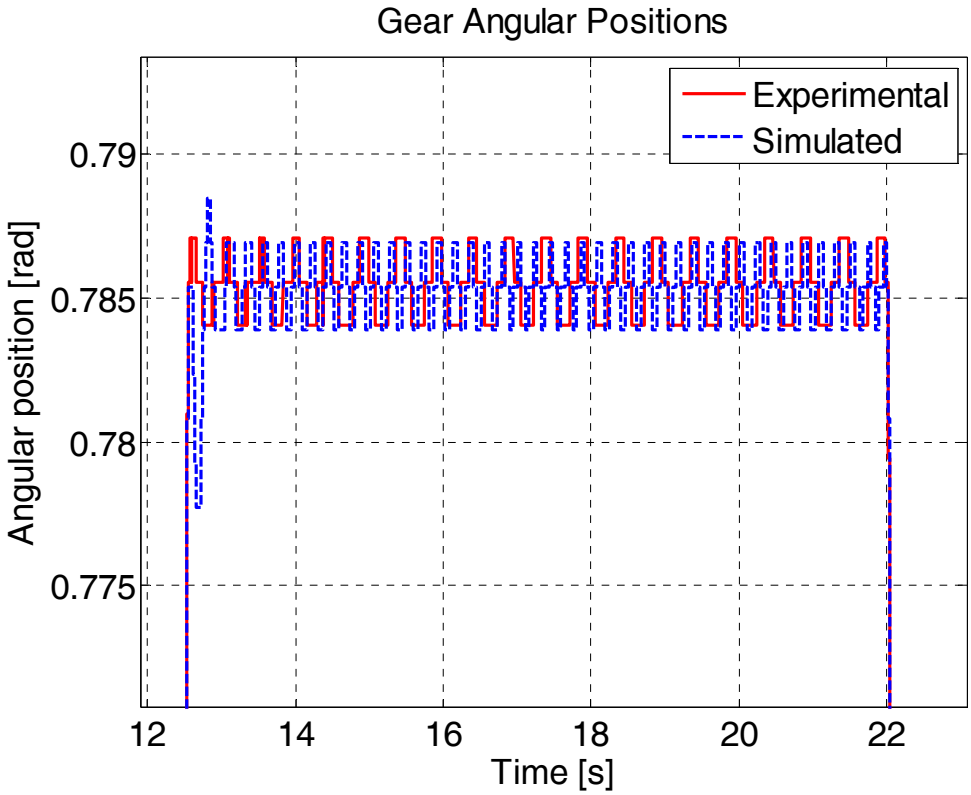

Figure 13 Gear set point achievement (enlargement of Figure 12).

The transient oscillation in Figure 13 is the same as in Figure 11 and would disappear by adding an appropriate known term $\underline{h}$ in the control law. To prove this, the measured angular position of the simulated and experimental runs are compared in Figure 13. The experimental measurement is free of the

transient oscillation because an appropriate $\underline{h}$ has been added to the control law for accounting viscous and static friction. The result highlights the different frequency bands where $\hat{d}_u$ and $\underline{h}(\hat{\mathbf{x}}_c)$ counteract the plant uncertainty. Assuming that the 'anti-causal limit' holds, $\hat{d}_u$ is estimated within the sensitivity BW f_m in (30). On the contrary, $\underline{h}(\hat{\mathbf{x}}_c)$, depending on the controllable state $\hat{\mathbf{x}}_c$, is estimated within the control law BW f_c, which, in absence of command limitations, may approach the Nyquist frequency $f_{\max} = 0.5/T = 100$ Hz. The limit cycles in Figure 13 are different in their period because of a different static friction. Experimental measurements in Figure 13 certify that the design model is a faithful description of the real plant.

5. Conclusion

The error loop, i.e. the loop from model to tracking error, points out which is the key design tool for accommodating uncertainties. The tool is the noise estimator, which is responsible for the noise estimates that update the disturbance state in the embedded model. Actually, causality constraint adds a further degree-of-freedom to the design, allowing the control law to play a role in making the design feasible, especially when contrasting stability and performance inequalities need to be satisfied. Employing asymptotic expansions of the closed-loop transfer functions, simple and explicit design formulae relating closed-loop eigenvalues to model parameters and requirements have been derived. Refinement may be pursued through simulation and in field.

Acknowledgments

The paper is a revised and expanded version of a paper entitled "The error loop and robust closed-loop stability", presented at IEEE ICMA 2012 Conference, Chengdu, August 5-8, 2012.

References

[1] J. Maciejowski, *Multivariable feedback design*, Addison Wesley, 1989.
[2] J. C. Doyle, B. A. Francis and A. R. Tannenbaum, *Feedback control theory*, Macmillan Pu. Co., New York, 1992.
[3] E. Canuto, A. Molano and L. Massotti "Drag-free control of the GOCE satellite: noise and observer design", *IEEE Trans. on Control Systems Technology*, Vol. 18, No. 2, pp. 501-509, 2010.
[4] C. Johnson "Accommodation of external disturbances in linear regulator and servomechanism problems", *IEEE Trans. on Automatic Control*, Vol. 16, No. 6, pp. 635–644, 1971.
[5] G. Hostetter and J. Meditch "On the generalization of observers to systems with unmeasurable, unknown inputs" *Automatica*, Vol. 9, No. 6, pp. 721-724, 1973.
[6] T. Mita, M. Hirata, K. Murata and H. Zhang "H_∞ control versus disturbance-observer-based control", *IEEE Trans. on Industrial Electronics*, Vol.45, No. 3, pp. 488-495, 1998.
[7] R. Bickel and M. Tomizuka, "Passivity-based versus disturbance observer based robot control: equivalence and stability," *ASME J. Dynamic. Systems, Measurement, and Control*, Vol. 121, No. 1, pp. 41-47, 1999.
[8] E. Schrijver and J. van Dijk, "Disturbance observers for rigid mechanical systems: Equivalence, stability, and design," *ASME J. Dynamic Systems, Measurement, and Control*, Vol. 124, No. 4, pp. 539-548, 2002.
[9] Y. Choi, K. Yang, W. K. Chung, H. R. Kim, and I. H. Suh, "On the robustness and performance of disturbance observers for second-order systems," *IEEE Trans. on Automatic Control*, Vol. 48, No. 2, pp. 315-320, 2003.
[10] S. Katsura, Y. Matsumoto and K. Ohnishi, "Modelling of force sensing and validation of disturbance observer for force control", *IEEE Trans. on Industrial Electronics,* Vol. 54, No. 1, pp. 530-538, 2007.
[11] E. Canuto, "Embedded Model Control: outline of the theory", *ISA Transactions,* Vol. 46, No. 3, pp. 363-377, 2007.
[12] F. Donati and M. Vallauri, "Guaranteed control of 'almost-linear' plants", *IEEE Trans. on Automatic Control*, Vol. 29, No. 1, pp. 34-41, 1984.
[13] H. Chapellat, M. Dahleh, and S. P. Bhattacharyya "Robust stability under structured and unstructured perturbations", *IEEE Trans. on Automatic Control,* Vol. 35, No. 10, pp. 1100-1108, 1990.
[14] Y. K. Foo and Y.C. Soh "Robust stability bound for systems with structured and unstructured perturbations", *IEEE Trans. on Automatic Control*, Vol. 38, No. 7, pp. 1150-1154, 1993.
[15] B. Ross Barmish, *New tools for robustness of linear systems*, Macmillan Pu. Co., New York, 1994.
[16] G. Calafiore and F. Dabbene, "A probabilistic framework for problems with real structured uncertainty in system and control", *Automatica*, Vol. 38, No. 8, pp. 1265-1276, 2002.
[17] P.M. Patre, W. MacKunis, C Makkar and W.E. Dixon "Asymptotic tracking for systems with structured and unstructured uncertainties", *IEEE Trans. on Control Systems Technology*, Vol. 16, No. 2, pp. 373-379, 2008.

[18] S.-H. Chen, J.-H. Chou and L.-A. Zheng, "Stability robustness of linear output feedback systems with time-varying structured and unstructured parameter uncertainties as well as delayed perturbations", *J. Franklin Institute,* Vol. 342, No. 2, pp. 213-234, 2005.
[19] E. Canuto, W. Acuna Bravo, A. Molano, C. Perez C. "Embedded Model Control calls for disturbance modeling and rejection," *ISA Transactions*, Vol. 51 No. 5, pp. 584-595, 2012.
[20] H. Kwakernaak and R. Sivan, *Linear optimal control systems*. J. Wiley & Sons, 1972.
[21] M. I. Solihin, R. Akmeliawati and A. Legowo "Robust feedback control design using PSO-based optimization: a case study in gantry crane control", *Int, J. of Mechatronics and Automation,* Vol. 1, No. 2, pp. 121-131, 2011.
[22] E. Canuto and A. Rolino "Multi-input digital frequency stabilization of monolithic lasers", *Automatica*, Vol. 40, No. 12, pp. 2139-2147, 2004,
[23] E. Canuto, "Drag-free and attitude control for the GOCE satellite", *Automatica*, Vol. 44, No. 7, pp 1766-1780, 2008.
[24] C. Canudas de Wit, H. Olsson, K. J. Åström and P. Lischinsky, "A new model for control of systems with friction", *IEEE Trans. on Automatic Control,* Vol. 40, No. 3, pp. 419-425, 1995.
[25] M. Keshmiri, A. F. Jahromi, A. Mohebbi, M.H. Amoozgar and W-F. Xie "Modelling and control of a ball and beam system using model based and non-model based control approaches", *Int. J. on Smart Sensing and Intelligent Systems,* Vol. 5. No.1, pp. 14-35, 2012.
[26] E. F. Camacho and C. Bordons, *Model Predictive Control*. Springer Verlag, London, 2003.
[27] B.-F. Wu and E.A. Jonckheere "A simplified approach to Bode's theorem for continuous-time and discrete-time systems", *IEEE Trans. on Automatic Control*, Vol. 37, No. 11, pp. 1797-1802, 1992.
[28] C. Desoer and M. Vidyasagar, *Feedback systems: input-output properties*. Academic Press, New York, 1975.